Journal of Materials Chemistry C

Photons and charges from colloidal doped semiconductor quantum dots

Journal:	*Journal of Materials Chemistry C*
Manuscript ID	TC-REV-09-2019-005150.R1
Article Type:	Review Article
Date Submitted by the Author:	23-Oct-2019
Complete List of Authors:	Qiao, Tian; Texas A&M University College Station, Department of Chemistry Parobek, David; Texas A&M University College Station, Department of Chemistry Son, Dong Hee; Texas A and M University College Station, Department of Chemistry

Photons and charges from colloidal doped semiconductor quantum dots

Tian Qiao[1], David Parobek[1] and Dong Hee Son[1,2, a)]

[1]Department of Chemistry, Texas A&M University, College Station, Texas 77843, USA

[2]Center for Nanomedicine, Institute for Basic Science (IBS), Seoul 03722, Republic of Korea

[a)] Electronic address: dhson@chem.tamu.edu

Abstract

The utility of colloidal semiconductor quantum dots as a source of photons and charge carriers for photonic and photovoltaic applications has created a large field of research focused on tailoring and broadening their functionality beyond what the exciton can provide. One approach towards expanding the range of characteristics of photons and charge carriers from quantum dots is through doping impurity ions (e.g. Mn^{2+}, Cu^{+}, and Yb^{3+}) in the host quantum dots. In addition to the progress in the synthesis enabling the fine control of the structure of the doped quantum dots, mechanistic understanding of the underlying processes correlated with the structure has been crucial in revealing the full potential of the doped quantum dots as the source of photons and charge carriers. In this review, we discuss recent progresses made in gaining microscopic understanding of the photophysical pathways that give rise to unique dopant-related luminescence and the generation of energetic hot electrons via exciton-to-hot electron upconversion.

1. Introduction

The primary function of the colloidal semiconductor quantum dots (QDs) in most of their applications is as the source of photons[1-3] or charge carriers.[4-6] Therefore, much effort was put into the research on controlling the characteristics of photons and charge carriers and improving the efficiency of generating them. For instance, the capability to control the wavelength, polarization and even direction of photon emission of the photons in the individual and the ensemble of the QDs were sought after in addition to seeking the higher emission quantum yield when using them as the source of photons. As the source of charge carriers, producing and extracting the electrons and holes with sufficient energy to perform the electrochemical or electrical work with maximum efficiency is the main interest. In addition to varying the material itself, several other strategies have been used to achieve these, including quantum confinement, [7-9] anisotropic morphology,[10-12] surface modification[13-15] and heterostructure formation.[16, 17]

Doping of the QDs with certain metal ions has been explored extensively to expand the range of characteristics of photons and charge carriers beyond what can be achieved by changing the host nanocrystal structure and interfacial ligand chemistry.[18-20] For instance, isoelectronic doping of Mn^{2+} ions to replace the divalent metal ions in binary and ternary QDs resulted in the sensitized photoluminescence originating from the ligand field transition of Mn^{2+} in addition to the exciton luminescence.[21-24] Doping of other metal ions such as Cu^{+} [19] and Ag^{+} [25, 26] were also shown to introduce new photon emission pathways or alter the competition between the radiative and nonradiative recombination of exciton in the host QDs. Doping of Mn^{2+} ions has been recently shown to open new pathways that can produce energetic hot electrons via exciton-to-hot electron upconversion process, enabling hot electron-induced photochemistry.[27-29] Some reports also suggested the possibility of Mn being the acceptor and donor of electron in Mn-doped QDs, relaying the electron between the conduction band and its final destination.[30]

In this article, we will discuss the progress made in controlling the characteristics of photons and charge carriers produced in QDs via doping of cations with emphasis on highlighting the developments in recent years. We will use the word colloidal QDs throughout this article in a broad and relaxed sense to represent the semiconductor nanocrystals in general including not only the quantum confined 0-dimensional nanocrystals but also those with very weak confinement effect. This article has two main Sections discussing the control of the properties of photons and charge carriers by doping. Section 2 discusses non-exciton luminescence resulting from doping of the

QDs via different mechanisms that depend on the identity of the dopant ions. Section 3 discusses the mechanism of producing hot electrons in Mn-doped QDs via biphotonic exciton-to-hot electron upconversion process and the detection of hot electrons. The later part of Section 3 makes comments on the potential function of Mn dopant as the electron acceptor and donor that has been suggested in the literature as the origin of the enhanced photovoltaic performance in the QD-sensitized solar cells.

2. Photons from doped quantum dots

In this section, we will discuss the luminescence in several metal ion-doped semiconductor quantum dots (QDs), where the new radiative photophysical pathways introduced by the dopant produce new luminescence in addition to exciton luminescence of the host QDs. While doping can also modify exciton luminescence of the host, for instance by creating strong effective magnetic field under the external field,[31] the present review will focus on the new luminescence not originating from the exciton. Here, we will introduce QDs doped with three different prototypical dopants that emit photons through the following three distinct photophysical pathways that have been attracting much attention: dopant sensitization, recombination involving charge carrier localized on dopant, and quantum cutting. When the QDs are doped with more than one type of dopant, the competition among different photon emitting pathways creates more diverse luminescence.[32]

2.1 Sensitization of dopant

Mn-doped QDs are among the most comprehensively studied doped QDs for its strong sensitized luminescence that arises from the ligand field transition of Mn^{2+} ions. Due to its relatively high luminescence quantum yield and large Stokes shift compared to the exciton luminescence, Mn luminescence has been extensively utilized in various applications including light emitting devices, bioimaging and solar concentrators.[18, 33-37]

Intense sensitized Mn luminescence occurs via efficient energy transfer from the exciton to Mn^{2+} ions when the bandgap of the host QDs is sufficiently large to drive net unidirectional energy transfer from the exciton to the dopant as depicted in Fig. 1a. Because the energy of the ligand field transition is determined by the strength of the ligand field dictated by the coordination structure around Mn^{2+} ions, Mn luminescence energy is not as sensitive to the variation of the chemical identity of the host QD and its size and morphology, unlike the exciton luminescence.[38]

Therefore, most of Mn-doped QDs exhibit luminescence of similar color centered around 600 nm with relatively small variation (a few tens of nm) of the peak wavelength as shown in Fig. 1b. The variation of the energy and the lifetime of Mn luminescence in different Mn-doped QDs reflects the difference in the strength of the ligand field, spin-orbit coupling and inter dopant exchange interaction.[39] So far, Mn doping in QDs has been reported in various binary and ternary systems as listed in Table 1, all of which exhibit orange-colored Mn luminescence when exciton-Mn energy transfer is allowed. Earlier synthetic efforts were focused on doping binary II-VI semiconductor QDs while the range of host QDs is expanding to ternary systems including $CuInS_2$ and lead halide perovskite QDs.

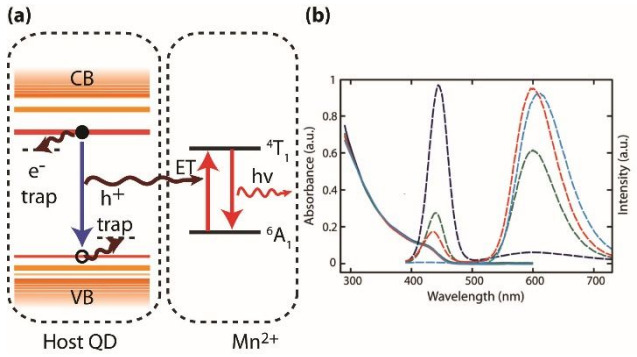

Fig. 1 (a) Energy transfer (ET) pathway in Mn-doped QDs. Energy transfer is competing with exciton recombination and electron/hole trapping. (b) Absorption (solid line) and photoluminescence (dashed line) spectra of Mn-doped CdS/ZnS core/shell QDs with varying doping concentrations. Reproduced with permission from ref 98. Copyright American Chemical Society (2010).

Table 1. Host materials for Mn-doped semiconductor QDs.

II-VI semiconductors	ZnO,[40] ZnS,[41-44] ZnSe,[45-48] CdS,[42, 48, 49] CdSe,[31, 50-54] CdTe,[48] ZnCdS,[55] CdSeTe[56, 57]
	CdS/ZnS,[58-61] ZnSe/CdSe/ZnSe,[62] CdSSe/ZnS,[63] ZnSe/ZnCdSe,[64] ZnSe /ZnS/CdS/ZnS,[65] CdS/ZnSe/ZnS[66]
Lead halide perovskites	$CsPbCl_3$,[67-73] $CsPb(Cl/Br)_3$,[67, 74-76] $CsPbBr_3$,[73, 77, 78] $CsPbI_3$,[79, 80] $CH_3NH_3PbCl_3$[81]
Other semiconductors	PbSe,[82] InAs,[83] Ag-In-Zn-S,[84] Zn-Cu-In-S,[85] Zn-In-S[86]
	InP/ZnS,[87] Zn-Cu-In-S/ZnS,[88] Zn-In-S/ZnS[89]

The quantum yield (QY) of Mn luminescence can be very high (~90 %) when the appropriate host QD and doping concentration are chosen, indicating the efficient energy transfer favorably competing with other processes.[60] As in the case of undoped QDs, trapping of electron or (and) hole is the major pathway that depletes the exciton population nonradiatively (Fig. 1a), although the trapped charge carriers can exhibit lower-energy trap emission.[90-92] The type of interaction that mediates the exciton-Mn energy is the exchange interaction between exciton and *d* electron of Mn^{2+} ions, since the dipole-coupled energy transfer is inefficient due to the weak transitions between the ground state and the manifold of the excited ligand field states of Mn^{2+} ion in the lattice.[93] Since the strength of the exchange interaction depends on the wavefunction overlap between the donor and acceptor, the rate of energy transfer is strongly dependent on the relative location of the dopant within the host QD and doping concentration especially for the strongly quantum confined QDs.[60]

The earlier studies estimated the rate of exciton-Mn energy transfer from the radiative and nonradiative decay rates of exciton and luminescence quantum yields.[94-97] On the other hand, such indirect approach can be inaccurate especially when the ensemble of doped QDs are kinetically heterogeneous, where the average luminescence lifetime and average luminescence QY are not compatible with the rate equations describing the kinetically homogeneous system. More reliable exciton-Mn energy transfer rate was obtained from the direct time-resolved measurement employing the pump-probe transient absorption spectroscopy.[98] Using this approach, the rate of exciton-Mn energy transfer in Mn-doped CdS/ZnS core/shell QDs were measured by analyzing the difference in the bleach recovery dynamics of exciton transition in undoped and Mn-doped QDs of the same host structure as a function of the doping concentration and radial doping location within the QD.[60] This study showed that the energy transfer rate increases with increasing doping concentration for a given radial doping location from increasing overlap of the exciton wavefunction with dopant (Fig. 2). Depending the doping concentration and location, the energy transfer time in Mn-doped CdS/ZnS QDs varied in the range of 4-80 ps. In this system, hole trapping that was identified as the main nonradiative competing channel occurred on 50-100 ps time scale. The rapid exciton-Mn energy transfer compared to the exciton recombination and charge carrier trapping combined with inefficient nonradiative decay of the excited ligand field state of Mn^{2+} ion is the reason why Mn luminescence QY in Mn-doped QDs can be higher than exciton luminescence QY in the undoped QDs. In the case of Mn-doped lead halide perovskite

QDs that have been successfully synthesized in recent years, exciton-Mn energy transfer rate was measured in Mn-doped $CsPbCl_3$ QDs via pump-probe transient absorption measurements.[99] Energy transfer rate in Mn-doped $CsPbCl_3$ QDs was somewhat slower than in Mn-doped CdS/ZnS QDs, although more accurate comparison between the two systems of the same QD size and dopant distribution within the QD has yet to be made. At the doping concentration of 0.4%, Mn-doped $CsPbCl_3$ NCs exhibited the energy transfer time of 380 ps, which is 2-5 time slower than Mn-doped CdS/ZnS QDs of comparable doping structure.[99]

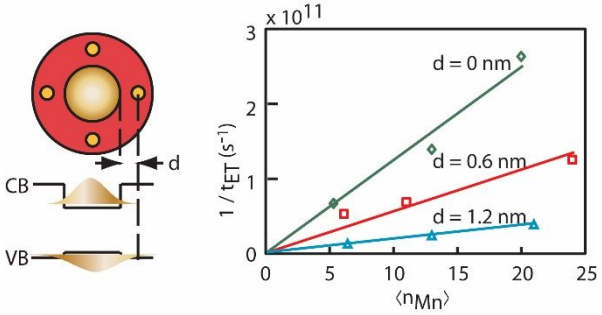

Fig 2. Doping location and concentration dependent energy transfer rate constant of Mn-doped CdS/ZnS QDs. For a given doping concentration, energy transfer rate increases as Mn^{2+} ions doped closer to the core. Energy transfer rate increases linearly to the doping concentration at a given radial doping location. $\langle n_{Mn} \rangle$ is the average number of Mn^{2+} ions doped in each QD. Reproduced with permission from ref 60. Copyright American Chemical Society (2011).

It is worth mentioning that the trapping of the electron or hole that usually inhibits exciton-Mn energy transfer can in some cases still enable the energy transfer from the 'trapped exciton' state to Mn^{2+} ions depending on the nature of the charge carrier trap. For example, introducing hole-trapping organic thiols as the surface-binding ligand to Mn-doped CdS/ZnS QDs has been shown to increase Mn luminescence intensity despite the fact that the same thiol ligand results in the quenching of exciton PL in undoped QDs via hole trapping.[100] This indicates that certain trapped exciton can be recovered as the sensitized Mn luminescence, although the energy transfer rate from the trapped exciton is significantly slower than the rate of 'normal' exciton-Mn energy transfer. The partial involvement of trapped exciton in the energy transfer has also been observed in the CdS/ZnS QDs codoped with Mn^{2+} and Ag^{+}, where doping of Ag^{+} can create the trapped exciton.[26]

As the bandgap of the host QDs becomes closer to the energy of Mn ligand field transition involved in the energy transfer, the initially net unidirectional energy transfer begins to experience

back energy transfer from the dopant to the host QD. In this case, the relative intensity of exciton and Mn luminescence varies depending on the donor-acceptor energy difference and temperature. The feeding from the long-lived emitting state of Mn^{2+} ($^4T_1$) back to the host to populate the exciton state also results in net elongation of the decay time of the exciton luminescence.[101] The robust dependence of the ratio of exciton and Mn luminescence intensities on the temperature, which is determined by the thermal equilibrium between the two states, has also been proposed for luminescence-based temperature sensing.[64, 102, 103]

As mentioned briefly earlier in this section, the spectral characteristics of Mn luminescence can be varied within a relatively narrow range by modifying the strength and structure of the ligand field or the extent of inter-dopant exchange coupling. For a given coordinating anion around Mn^{2+}, hydrostatic pressure or local lattice strain resulting from the lattice mismatch at the heterointerface alters the Mn luminescence energy by changing the ligand field strength.[61, 104] With increasing pressure, Mn luminescence energy decreased.[104] In addition, the signature of softening the local vibrational mode coupled to Mn ligand field transition was also observed when dopants are located close to the core/shell interface that imposes anisotropic lattice strain in Mn-doped CdS/ZnS QDs.[105] When Mn^{2+} ions experience the stronger lattice strain, the spectral linewidth of Mn luminescence exhibited the higher sensitivity to the temperature, which was explained by the lower frequency of the local vibrational mode coupled to Mn ligand field transition compared to the bulk phonon of the host lattice. With increasing Mn-doping concentration, inter-dopant antiferromagnetic coupling becomes more significant resulting in the shortening of Mn luminescence lifetime.[45, 106]

The advantage of Mn-doped QDs as the source of photons in various applications compared to undoped QDs come from the large Stokes shift of dopant emission and multi-color emission whose intensity ratio can be used as sensing modality. For example, the absence of self-absorption of Mn luminescence is ideal for the application of Mn-doped QDs as the solar downconverter and concentrator with low loss. [107, 108] The sensitivity of relative ratio of exciton and Mn emission to chemical environment or temperature was utilized as the chemical or temperature sensing. [65]

2.2 Recombination of charge carrier localized on dopant

Another avenue producing new luminescence in doped QDs is by introducing dopants that function as the charge carrier recombination center, where one of the charge carriers localized on

or near the dopant radiatively recombines with the remaining charge carrier. Among the doped QDs that can exhibit the luminescence via dopant-centered charge carrier recombination, Cu-doped II-VI QDs were the most extensively studied. The dopants that can produce the luminescence via similar mechanism includes Ag^{+}, Cr^{3+} and Ni^{2+}, while they have not been explored as extensively as Cu dopant.[20] In contrast to Mn luminescence, the energy of Cu luminescence varies widely depending on the host QDs, e.g., 3 eV in Cu-doped ZnS QD and 0.9 eV in $Cu_2ZnSn(S_{1-x}Se_x)_4$ QD.[109, 110] The Cu luminescence decays on μs time scale, because it involves the recombination of the localized charge carrier exhibiting much lower oscillator strength than the delocalized exciton.[19]

Earlier literature discussing the luminescence from Cu-doped QDs had two different views on the oxidation state of the dopant between Cu^{+} [111-114] and Cu^{2+},[115-117] which fueled many detailed studies to identify the oxidation state of the dopant. Various optical,[114, 118] electron spin resonance,[119, 120] X-ray absorption spectroscopic[112, 121-123] and computational studies[124] were performed to clarify this issue. While we will not cover the full scope of the recent progress on this issue here, which are discussed in detail in a recent review,[19] we briefly highlight the key arguments supporting each view.

Studies by Gamelin and coworkers described the Cu luminescence as coming from QDs doped with Cu^{+}, where the rapid localization of the hole by Cu^{+} after the photoexcitation of exciton results in the radiative recombination of the localized hole with the remaining electron.[114] (Fig, 3a) In this picture, the initial hole localization on Cu^{+} produces Cu^{2+} like state, which returns back to Cu^{+} through the recombination with the electron giving rise to Cu luminescence.[114] The authors supported Cu^{+} state of the dopant in Cu-doped QDs by comparing the calculated absorption spectra of Cu^{+}- and Cu^{2+}-doped CdSe clusters (Cu^{+}:$Cd_{33}Se_{34}$ and Cu^{2+}:$Cd_{33}Se_{34}$).[124] In their work, they argued that only Cu^{2+}:$Cd_{33}Se_{34}$ exhibit distinct valence band-to-metal electron transfer transition extending into the near infrared (NIR) region at < 1eV, which has been experimentally observed in bulk ZnS doped with Cu^{2+} but not in Cu-doped ZnS QDs. The authors also reported the observation of valence band-to-metal electron transfer in the transient absorption studies of Cu-doped CdSe/CdS core/shell QDs as a weak photoinduced absorption, fortifying the mechanism of forming a Cu^{2+} state through hole localization at Cu^{+} after photoexcitation.[118] In addition, the absorption peak at 2.7 eV in the calculated absorption spectrum of Cu^{+}:$Cd_{33}Se_{34}$, attributed to the transition of the electron in Cu^{+} to the conduction band of the host. was observed experimentally

below the band to band transition in Cu-doped CdSe QDs.[114] These results were taken as a strong support for the argument that the oxidation state is Cu^{+} in Cu-doped QDs.

On the other hand, studies by Klimov and coworkers suggested that the dopant exists as Cu^{2+} in the QDs and acts as a permanent hole in the QD that recombines with the electron in the conduction band to produce the dopant luminescence and Cu^{+}. (Fig. 3b) [125] In their study, they reported magnetic circular dichroism (MCD) data of Cu-doped ZnSe/CdSe QDs showing an enhanced Zeeman splitting of 2.5 meV indicative of magnetic activity associated with Cu^{2+} with d^9 as opposed to Cu^{+} with d^{10} configuration of *d* electrons. On the other hand, this has been disputed by another study that reported the absence of electron paramagnetic resonance (EPR) signal and MCD from Cu-doped CdSe, InP and $CuInS_2$ QD, leaving room for further clarification.[114] The authors also observed the increase of Cu luminescence intensity when dodecanethiol was introduced to the Cu-doped ZnSe/CdSe QD surface, which acts as the hole trap that removes the hole produced in the valence band of the host after the photoexcitation.[125] This observation was interpreted as the result of the competition between the permanent hole on Cu^{2+} and the photogenerated hole in the valence band in the recombination with the electron in the conduction band, supporting Cu^{2+} dopant state. However, the absence of the channel regenerating Cu^{2+} state from Cu^{+} after charge carrier recombination that is required to sustain Cu luminescence under continued photoexcitation was pointed out as a weakness of Cu^{2+} scenario.[114]

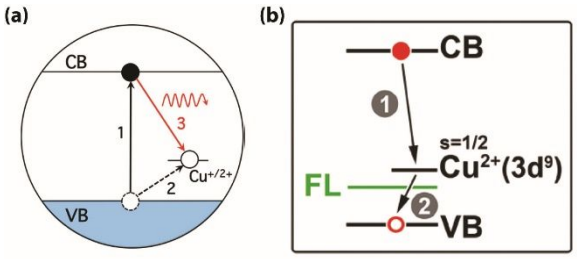

Fig. 3 (a) Copper dopant exists in the QDs as Cu^{+} that rapidly localizes a hole after the photoexcitation. The localized hole recombines with the electron to emit a photon. Reproduced with permission from ref 114. Copyright American Chemical Society (2015). (b) Copper dopant exists in the QDs as Cu^{2+} that acts as a permanent hole, which recombines with the electron to emit a photon. Reproduced with permission from ref 125. Copyright American Chemical Society (2011).

2.3 Downconversion by quantum cutting

Downconversion via quantum cutting has also been studied recently in lanthanide doped nanocrystals.[126-129] Quantum cutting that produces two lower-energy photons from one high-energy photon has been more frequently observed in insulating host materials doped with one or more types of lanthanide dopant ions that form a donor and acceptor pair.[130, 131] Often, the 'cutting' of one high-energy photon into two low-energy photons occurs by transferring the energy from one donor ion to the two acceptor ions, although the exact pathways of energy transfer varies depending on the identity of the lanthanide ions involved as illustrated in Fig. 4a.[132] For instance, in the Tb^{3+}-Yb^{3+} couple, Tb^{3+} is the donor and two Yb^{3+} ions are the acceptors represented by the case II of the scheme in Fig. 4a.[130]

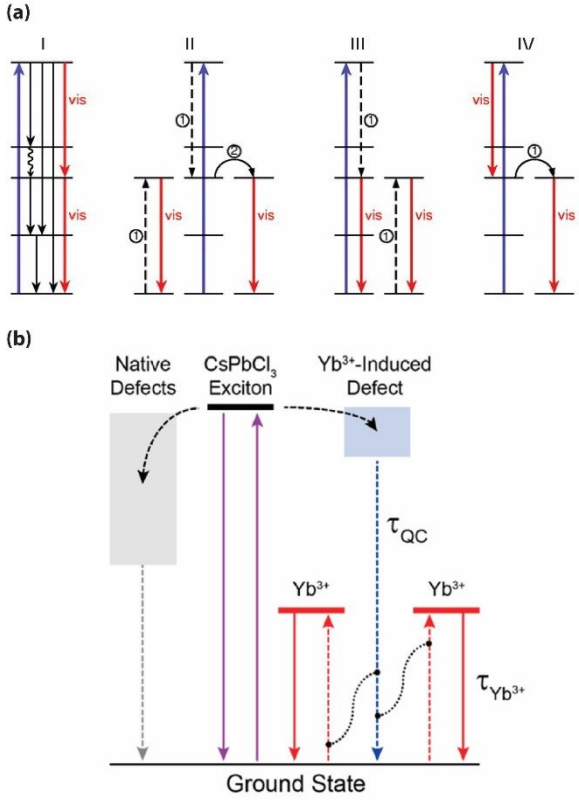

Fig. 4 (a) Energy level diagram showing the different pathways of quantum cutting involving lanthanide ions. Blue arrows indicate photoexcitation of lanthanide ions and red arrows indicate the emission of a downconverted photons. In case I, a single excited ion emits two photons sequentially. Quantum cutting can also occur via single-step (III and IV) or two-step (II) energy transfer to another lanthanide ion. Reproduced with permission from ref 132. Copyright The American Association for the Advancement of Science (1999). (b) Mechanism of Yb^{3+} sensitization in Yb-doped $CsPbCl_3$ QDs. Yb^{3+}-induced defect state localizes exciton and a pair of

Yb^{3+} are sensitized simultaneously by the trapped exciton. Reproduced with permission from ref 127. Copyright American Chemical Society (2018).

Recently, several groups reported the enhancement of quantum cutting efficiency by taking advantage of the sensitization by organic dyes or by using semiconductor QDs as the host matrix absorbing the high-energy photons efficiently.[126-129, 133] As the semiconductor host that can exhibit the enhanced quantum cutting, lead halide perovskite QDs have attracted much attention in recent years with the successful synthesis of lanthanide doped cesium lead halide ($CsPbX_3$) QDs. In the case of Yb-doped $CsPbCl_3$ QDs, downconversion of the visible light to near infrared (NIR) photons was achieved with the efficiency of up to 170 %.[127] In this case, the exciton initially excited in $CsPbCl_3$ QDs was considered to rapidly localize at the defects introduced by heterovalent doping as depicted in Fig. 4b. The subsequent energy transfer from the trapped exciton to the two adjacent Yb^{3+} ions produce two NIR photons at ~1.26 eV.

3. Charge carriers from Mn-doped quantum dots

While the role of dopant in tuning the spectral characteristics of the luminescence has been the main interest in many studies on doped QDs as discussed in the previous section, interest in altering the properties of the photoexcited charge carriers is also growing. Here, we will first discuss hot electron generation in Mn-doped QDs that takes advantage of the long-lived excited Mn ligand field state enabling the sequential 'upconversion' of two excitons into a pair of hot electron hole pair at low excitation intensities. In this process, the sensitized excited ligand field state of Mn^{2+} functions as the long-lived energy reservoir for the sequential resonant two-photon process. This process can be compared to the photon upconversion observed in many lanthanide doped nanocrystals except that higher-energy charge carrier is obtained instead of higher-energy photon.[134] In the later part of this section, we will discuss the feasibility of Mn dopant functioning as the electron storage and relay enhancing the charge collection efficiency in photovoltaic device platform that has been suggested in some literature.[30]

3.1 Hot electrons from doped quantum dots

Mn-doped QDs have received particular attention as the source of hot electrons from semiconductor QDs, since the long-lived ligand field state of Mn functions as the energy reservoir

playing a critical role as the intermediate state in producing hot electrons via sequential two photon process.[135, 136] Generation of hot electrons in Mn-doped QDs reported so far used II-VI QDs as the host while new platforms such as lead halide perovskite QDs are being pursued as a new host material. Because of their large excess kinetic energy, hot electrons exhibit superior electron transfer capability compared to the lower energy bandedge electrons. For this reason, hot electrons are actively pursued for various photophysical and photochemical applications such as in photovoltaics[27] and photocatalysis.[63]

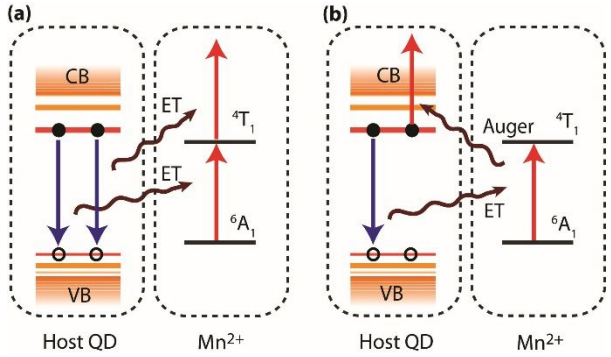

Fig. 5 Photophysical pathways that generate hot electrons in Mn-doped QDs. (a) Hot electrons are generated by consecutive exciton-to-Mn energy transfer. (b) Hot electrons are generated by exciton-to-Mn energy transfer followed by Auger type back energy transfer from Mn^{2+} to conduction band electron.

The mechanisms of producing hot electrons in Mn-doped QDs were proposed early during this decade and the experimental detection of hot electrons as the photocurrent in electrochemical cell, photodiode platform and also as photoelectron emission followed soon.[27-29, 135, 136] Fig. 5 shows the two proposed photophysical pathways that can generate highly energetic hot electrons.[135, 136] One is the two consecutive exciton-Mn energy transfer to the same Mn^{2+} as illustrated in Fig. 5a, which was proposed by the authors' group.[136] This produces highly excited Mn^{2+} ions that can give up the electron to the conduction band of the host with significant excess kinetic energy and recover Mn^{2+} oxidation state by creating a localized hole near the dopant. This mechanism was initially proposed from the observation of the decrease of the intensity of Mn luminescence from $^4T_1 \rightarrow {}^6A_1$ transition with increasing excitation rate due to the loss of the emitting $^4T_1$ population in

Mn-doped CdS/ZnS QDs. Another proposed pathway for the generation of hot electrons is the exciton-Mn energy transfer followed by Auger energy transfer from $^4T_1$ state of Mn^{2+} to the exciton excited by the second photon absorption as illustrated in Fig. 5b.[137] In this case, $^4T_1$ state of Mn^{2+} ion can transfer to either electron or hole. In the earlier work reported by Gamelin and coworkers, they observed the quenching of Mn luminescence upon the electrochemical injection of electron into the conduction band of the host, which was explained by the Auger deexcitation of $^4T_1$ state of Mn^{2+} ion by the injected electron.[137] If the Auger deexcitation of $^4T_1$ state of Mn^{2+} ion involves primarily the electron of the photoexcited electron rather than holes, the net result is the generation of hot electron in conduction band and delocalized hole in the valence band.

While it is not straightforward to tell which particular mechanism is dominating under a given condition, both pathways produce hot electrons with excess kinetic energy in the conduction band. On the other hand, the energy level of hot electrons and its dependence on the host bandedge level are different in the two cases. Since the hot electrons from pathway (b) are produced by transferring the energy from $^4T_1$ state of Mn^{2+} to the electrons in conduction band, the energy of hot electrons can be varied by tuning the host bandedge, whereas pathway (a) will produce hot electrons whose energy is insensitive to the host bandedge level. One important aspect of hot electron generation in Mn-doped QDs common to both pathways in Fig. 5 is the extremely long lifetime of $^4T_1$ state of Mn^{2+} that serves as the intermediate state for the sequential two-step process. Despite the fact that hot electron generation is biphotonic, it can occur at very low excitation intensity thanks to the long intermediate state lifetime. For >5 ms lifetime of $^4T_1$ state of Mn^{2+} doped in CdS/ZnS QDs, excitation intensities equivalent to the concentrated solar radiation was sufficient to produce hot electrons via the biphotonic upconversion process.[63]

The direct experimental verification of the generation of hot electrons was made in several different platforms. In the authors' group, hot electron photocurrent was first measured in a photoelectrochemical cell platform shown in Fig. 6a.[28] The anode is constructed by depositing CdS/ZnS QDs on an ITO substrate that has Al_2O_3 overlayer of varying thickness on top of ITO layer. Al_2O_3 is an insulating layer that provides a high energy barrier for the electrons near the edge of the conduction band. Only hot electrons with sufficient excess energy can tunnel through this insulating barrier. When undoped CdS/ZnS QDs that generate the electrons only near the conduction bandedge are deposited on the anode, no detectable photocurrent was observed. In contrast, anodes deposited with Mn-doped CdS/ZnS QDs exhibited photocurrent that increased

superlinearly with excitation intensity, which is consistent with the biphotonic hot electron generation mechanism as shown in Fig. 6b.

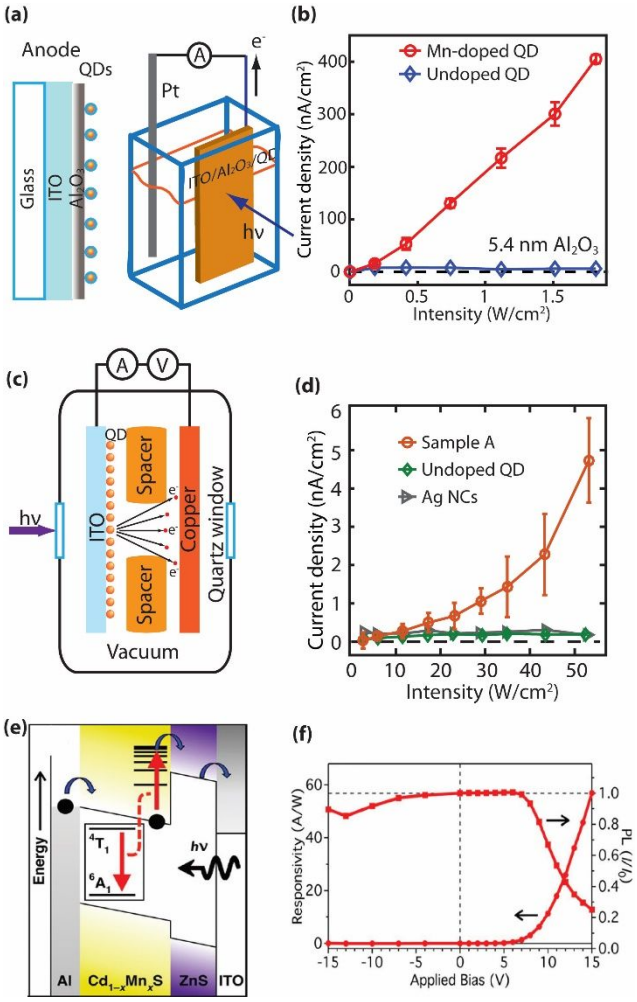

Fig. 6 (a) A photoelectrochemical cell constructed to detect hot electrons generated in Mn-doped CdS/ZnS QDs. (b) Comparison of hot electron photocurrent from Mn-doped CdS/ZnS QDs (red) and undoped CdS/ZnS QDs (blue). (a) and (b) are reproduced with permission from ref 28. Copyright John Wiley and Sons (2016). (c) Electrodes fabricated to detect photoelectron emission from Mn-doped CdS/ZnS QDs. (d) Comparison of the photoemission current density from Mn-doped CdS/ZnS QDs (red), undoped CdS/ZnS QDs (green) and Ag nanocrystals (grey). (c) and (d) are reproduced with permission from ref 29. Copyright American Chemical Society (2016). (e) A photodiode built to detect photocurrent from hot electrons. (f) Mn PL intensity and photodiode responsivity under different bias voltage. (e) and (f) are reproduced with permission from ref 27. Copyright American Chemical Society (2016).

Another study from the authors' group that showed the generation of hot electrons more directly was performed using the CdS/ZnS QD-coated ITO substrate as the source of photoelectrons under vacuum.[29] Fig. 6c shows the setup that measured the current from the photoelectron emission of hot electrons. In this experiment, while the average energy of hot electrons produced in Mn-doped CdS/ZnS QDs are below the vacuum level, a subset of hot electrons that exceeds the ionization threshold at the high-energy tail of the energy spectrum are emitted as the photoelectron. The photoelectron current densities measured at 0 V bias between the ITO and copper electrodes are compared between Mn-doped and undoped CdS/ZnS QDs in Fig. 6d. As expected from the biphotonic upconversion process for the generation of hot electrons, only Mn-doped CdS/ZnS QDs exhibit the hot electron photoemission current that increase approximately quadratically with the excitation intensity. For comparison, the measurement using Ag nanocrystals capable of producing plasmonic hot electrons under the same excitation condition is also made. In contrast to Mn-doped CdS/ZnS QDs, the energy level of hot electrons from Ag nanocrystals are too low to produce measurable photoemission current because the excess energy from the plasmon is used to promote the electron from below the Fermi level.

Detection of hot electrons in the photodiode platform was reported by Gamelin and coworkers.[27] Fig. 6e shows the energy level structure of each component layer in the photodiode structure used to measure hot electron photocurrent. In this photodiode structure, ZnS is the blocking layer that allows only the electrons with sufficient energy, i.e., hot electrons, to generate the photocurrent. The photocurrent was observed only when the electron was injected to the layer of Mn-doped CdS QDs under sufficiently positive bias as shown in Fig. 6f, so that Auger deexcitation of $^4T_1$ state of Mn^{2+} to the injected electron can produce hot electrons. Generation of hot electron photocurrent was also accompanied by the decrease of Mn luminescence as required by the mechanism of hot electron generation.

3.2 Possibility of Mn as the electron acceptor and donor

The possibility of Mn^{2+} ions in Mn-doped QDs to function as the acceptor and donor of 'electrons' has recently been discussed in the literature. Such possibility has been suggested from the observation of the increased photocurrent in the photovoltaic devices fabricated with Mn-doped QDs compared to those fabricated with undoped QDs.[138, 139] Mn dopant's possible electron relaying function has also been suggested to explain the slower recombination of the spatially

separated charge carriers in Mn-doped type-II core/shell quantum well structure compared to the undoped counterpart.[57] In these studies, the enhanced photocurrent or slower recombination of the charge carrier was attributed to the long-lived charge carriers, specifically electron, residing in a state created by Mn doping. In the study by Kamat and coworkers, the authors explained the increase of photocurrent and photovoltage from Mn doping in QD-sensitized solar cells with the electron-accepting midgap state formed by Mn doping while not being specific about the nature of the midgap state.[138] Other study performed in Mn-doped CdSe QD also reported the enhancement of photocurrent by Mn doping, indicating the involvement of some type of trap state that can hold the electron longer, therefore improving charge carrier collection efficiency.[139] On the other hand, some of the later studies interpreted such enhanced photocurrent as a result of the long lifetime of photogenerated charge carriers that reduces the electron hole-recombination, attributing the longevity of the carrier lifetime to the long lifetime of $^4T_1$ ligand field state.[140] However, such interpretation is problematic since $^4T_1$ state is created by the transfer of the energy of exciton (i.e., both electron and hole pair) not just electron to reduce the electron hole recombination. Some reports incorrectly portrayed $^4T_1$ ligand field state as the charge accepting level of Mn dopant that resides within the bandgap of the host that relays the electron from the conduction band of the host QD to other nanocrystals such as TiO_2 in the Mn-doped $CuInS_2$/CdS QD-sensitized solar cells.[141] In a study by Ghosh and coworkers, it was suggested that Mn^{2+} can be reduced to Mn^{1+} by capturing the electron from the conduction band of the host for a prolonged period and donate the electron back to the host, therefore performing the function of electron storage.[57] While doping of Mn^{2+} ions may potentially create a defect state near the dopant that can trap and detrap the electrons with effective elongation of electron lifetime, more conclusive evidence for the involvement of Mn^{2+}/Mn^{1+} redox process has yet to be acquired.

4. Conclusion and Outlook

We discussed modification of the characteristics of photons and charge carriers in photoexcited colloidal QDs by introducing dopants in the QD lattice that open new pathways of energy or charge flow. Compared to the exciton luminescence of the host QDs, dopant luminescence covers the larger spectral range for a given host QD by utilizing various radiative decay pathways that depends on the specific dopant present in the host. While the interest in doped QDs has been focused on the spectral tunability of the luminescence, doped QD is also a useful platform for

exploring the coupling among electronic, lattice and spin degrees of freedom. Through the magnetism carried by the dopant or its ability to localize the charge, one could gain additional control of the properties of photons emitted, which will further expand the functionality of the doped QDs as the source of photons. Hot electrons from the doped QDs are also attracting attention for their capability to perform more efficient electron transfer overcoming a high and wide energy barrier. Photocatalytic reduction is an example where the hot electrons can be particularly useful. Compared to the plasmonic hot electrons produced in metal nanocrystals, hot electrons from Mn-doped QDs is more energetic by several eV because of the biphotonic upconversion process using the energy of two excitons. The high energy of hot electrons even capable of being above the vacuum level combined with low required photoexcitation intensity for upconversion can open the door to practical utilization of energetic hot electrons for the photochemical process. The progress made in the control of the characteristics of photons and charges in doped QDs is the result of the combined efforts in developing the synthesis methodologies and in understanding the underlying principles at microscopic level, which will continue to be crucial for future research in this field.

Acknowledgements

This work was supported by National Science Foundation (CBET-1804412, T.Q., D. P.) and Institute for Basic Sciences (IBS-R026-D1, D.H.S.).

References

1. J. Caruge, J. Halpert, V. Wood, V. Bulović and M. Bawendi, *Nat. Photonics*, 2008, **2**, 247.
2. E. Jang, S. Jun, H. Jang, J. Lim, B. Kim and Y. Kim, *Adv. Mater. (Weinheim, Ger.)*, 2010, **22**, 3076-3080.
3. B. S. Mashford, M. Stevenson, Z. Popovic, C. Hamilton, Z. Zhou, C. Breen, J. Steckel, V. Bulovic, M. Bawendi and S. Coe-Sullivan, *Nat. Photonics*, 2013, **7**, 407.
4. A. Nozik, *Physica E: Low-dimensional Systems and Nanostructures*, 2002, **14**, 115-120.
5. P. V. Kamat, *J. Phys. Chem. C*, 2008, **112**, 18737-18753.
6. A. Swarnkar, A. R. Marshall, E. M. Sanehira, B. D. Chernomordik, D. T. Moore, J. A. Christians, T. Chakrabarti and J. M. Luther, *Science* 2016, **354**, 92-95.
7. F. W. Wise, *Acc. Chem. Res.*, 2000, **33**, 773-780.

8. D. J. Norris and M. Bawendi, *Phys. Rev. B*, 1996, **53**, 16338.
9. Y. Dong, T. Qiao, D. Kim, D. Parobek, D. Rossi and D. H. Son, *Nano Lett.*, 2018, **18**, 3716-3722.
10. X. Peng, L. Manna, W. Yang, J. Wickham, E. Scher, A. Kadavanich and A. P. Alivisatos, *Nature* 2000, **404**, 59.
11. Y. Dong, T. Qiao, D. Kim, D. Rossi, S. J. Ahn and D. H. Son, *Chem. Mater.*, 2019, **31**, 5655-5662.
12. S. Ithurria, M. Tessier, B. Mahler, R. Lobo, B. Dubertret and A. L. Efros, *Nat. Mater.*, 2011, **10**, 936.
13. B. A. Koscher, J. K. Swabeck, N. D. Bronstein and A. P. Alivisatos, *J. Am. Chem. Soc.*, 2017, **139**, 6566-6569.
14. O. Chen, J. Zhao, V. P. Chauhan, J. Cui, C. Wong, D. K. Harris, H. Wei, H.-S. Han, D. Fukumura, R. K. Jain and M. G. Bawendi, *Nat. Mater.*, 2013, **12**, 445.
15. C. Pu and X. Peng, *J. Am. Chem. Soc.*, 2016, **138**, 8134-8142.
16. S. Kim, B. Fisher, H.-J. Eisler and M. Bawendi, *J. Am. Chem. Soc.*, 2003, **125**, 11466-11467.
17. K. Wu and T. Lian, *Chem. Soc. Rev.*, 2016, **45**, 3781-3810.
18. D. J. Norris, A. L. Efros and S. C. Erwin, *Science* 2008, **319**, 1776-1779.
19. K. E. Knowles, K. H. Hartstein, T. B. Kilburn, A. Marchioro, H. D. Nelson, P. J. Whitham and D. R. Gamelin, *Chem. Rev.* , 2016, **116**, 10820-10851.
20. S. Jana, G. Manna, B. B. Srivastava and N. Pradhan, *Small*, 2013, **9**, 3753-3758.
21. A. K. Guria, S. K. Dutta, S. Das Adhikari and N. Pradhan, *ACS Energy Lett.*, 2017, **2**, 1014-1021.
22. H.-Y. Chen and D. H. Son, *Isr. J. Chem.*, 2012, **52**, 1016-1026.
23. R. Beaulac, P. I. Archer, S. T. Ochsenbein and D. R. Gamelin, *Adv. Funct. Mater.*, 2008, **18**, 3873-3891.
24. Y. Dong, D. Parobek and D. H. Son, *J. Korean Ceram. Soc.*, 2018, **55**, 515-526.
25. A. Sahu, M. S. Kang, A. Kompch, C. Notthoff, A. W. Wills, D. Deng, M. Winterer, C. D. Frisbie and D. J. Norris, *Nano Lett.*, 2012, **12**, 2587-2594.
26. W. Lee, J. Oh, W. Kwon, S. H. Lee, D. Kim and S. Kim, *Nano Lett.*, 2018, **19**, 308-317.
27. C. J. Barrows, J. D. Rinehart, H. Nagaoka, D. W. deQuilettes, M. Salvador, J. I. Chen, D. S. Ginger and D. R. Gamelin, *J. Phys. Chem. Lett.*, 2016, **8**, 126-130.
28. Y. Dong, D. Rossi, D. Parobek and D. H. Son, *ChemPhysChem*, 2016, **17**, 660-664.
29. Y. Dong, D. Parobek, D. Rossi and D. H. Son, *Nano Lett.*, 2016, **16**, 7270-7275.
30. T. Debnath and H. N. Ghosh, *J. Phys. Chem. C*, 2019, **123**, 10703-10719.
31. R. Beaulac, L. Schneider, P. I. Archer, G. Bacher and D. R. Gamelin, *Science* 2009, **325**, 973-976.
32. S. Jana, B. B. Srivastava and N. Pradhan, *J. Phys. Chem. Lett.*, 2011, **2**, 1747-1752.
33. S. C. Erwin, L. Zu, M. I. Haftel, A. L. Efros, T. A. Kennedy and D. J. Norris, *Nature* 2005, **436**, 91-94.
34. C. Wei, Z. Z. Jin and G. J. Alan, *J. Nanosci. Nanotechnol.*, 2004, **4**, 919-947.
35. R. Beaulac, P. I. Archer and D. R. Gamelin, *J. Solid State Chem.*, 2008, **181**, 1582-1589.
36. D. D. Sarma, R. Viswanatha, S. Sapra, A. Prakash and M. Garcia-Hernandez, *J. Nanosci. Nanotechnol.*, 2005, **5**, 1503-1508.
37. H. Yang, S. Santra and P. H. Holloway, *J. Nanosci. Nanotechnol.*, 2005, **5**, 1364-1375.
38. N. Pradhan, D. M. Battaglia, Y. Liu and X. Peng, *Nano Lett.*, 2007, **7**, 312-317.

39. D. Boulanger, R. Parrot and Z. Cherfi, *Phys. Rev. B*, 2004, **70**, 075209.
40. N. S. Norberg, K. R. Kittilstved, J. E. Amonette, R. K. Kukkadapu, D. A. Schwartz and D. R. Gamelin, *J. Am. Chem. Soc.*, 2004, **126**, 9387-9398.
41. R. N. Bhargava, D. Gallagher, X. Hong and A. Nurmikko, *Phys. Rev. Lett.*, 1994, **72**, 416-419.
42. M. Azad Malik, P. O'Brien and N. Revaprasadu, *J. Mater. Chem.*, 2001, **11**, 2382-2386.
43. E. Sotelo-Gonzalez, L. Roces, S. Garcia-Granda, M. T. Fernandez-Arguelles, J. M. Costa-Fernandez and A. Sanz-Medel, *Nanoscale*, 2013, **5**, 9156-9161.
44. B. B. Srivastava, S. Jana, N. S. Karan, S. Paria, N. R. Jana, D. D. Sarma and N. Pradhan, *J. Phys. Chem. Lett.*, 2010, **1**, 1454-1458.
45. J. F. Suyver, S. F. Wuister, J. J. Kelly and A. Meijerink, *Phys. Chem. Chem. Phys.*, 2000, **2**, 5445-5448.
46. D. J. Norris, N. Yao, F. T. Charnock and T. A. Kennedy, *Nano Lett.*, 2001, **1**, 3-7.
47. N. Pradhan, D. Goorskey, J. Thessing and X. Peng, *J. Am. Chem. Soc.*, 2005, **127**, 17586-17587.
48. V. A. Vlaskin, C. J. Barrows, C. S. Erickson and D. R. Gamelin, *J. Am. Chem. Soc.*, 2013, **135**, 14380-14389.
49. L. Levy, J. F. Hochepied and M. P. Pileni, *J. Phys. Chem.*, 1996, **100**, 18322-18326.
50. F. V. Mikulec, M. Kuno, M. Bennati, D. A. Hall, R. G. Griffin and M. G. Bawendi, *J. Am. Chem. Soc.*, 2000, **122**, 2532-2540.
51. D. Magana, S. C. Perera, A. G. Harter, N. S. Dalal and G. F. Strouse, *J. Am. Chem. Soc.*, 2006, **128**, 2931-2939.
52. J. Kobak, T. Smoleński, M. Goryca, M. Papaj, K. Gietka, A. Bogucki, M. Koperski, J. G. Rousset, J. Suffczyński, E. Janik, M. Nawrocki, A. Golnik, P. Kossacki and W. Pacuski, *Nat. Commun.*, 2014, **5**, 3191.
53. R. Fainblat, C. J. Barrows, E. Hopmann, S. Siebeneicher, V. A. Vlaskin, D. R. Gamelin and G. Bacher, *Nano Lett.*, 2016, **16**, 6371-6377.
54. W. Zheng, Z. Wang, J. Wright, B. Goundie, N. S. Dalal, R. W. Meulenberg and G. F. Strouse, *J. Phys. Chem. C*, 2011, **115**, 23305-23314.
55. A. Hazarika, A. Layek, S. De, A. Nag, S. Debnath, P. Mahadevan, A. Chowdhury and D. D. Sarma, *Phys. Rev. Lett.*, 2013, **110**, 267401.
56. J. Wang, Y. Li, Q. Shen, T. Izuishi, Z. Pan, K. Zhao and X. Zhong, *J. Mater. Chem.*, 2016, **4**, 877-886.
57. T. Debnath, S. Maiti and H. N. Ghosh, *J. Phys. Chem. Lett.*, 2016, **7**, 1359-1367.
58. Y. Yang, O. Chen, A. Angerhofer and Y. C. Cao, *J. Am. Chem. Soc.*, 2006, **128**, 12428-12429.
59. Y. Yang, O. Chen, A. Angerhofer and Y. C. Cao, *J. Am. Chem. Soc.*, 2008, **130**, 15649-15661.
60. H.-Y. Chen, S. Maiti and D. H. Son, *ACS Nano*, 2012, **6**, 583-591.
61. E. Hofman, R. J. Robinson, Z.-J. Li, B. Dzikovski and W. Zheng, *J. Am. Chem. Soc.*, 2017, **139**, 8878-8885.
62. A. Hazarika, A. Pandey and D. D. Sarma, *J. Phys. Chem. Lett.*, 2014, **5**, 2208-2213.
63. Y. Dong, J. Choi, H.-K. Jeong and D. H. Son, *J. Am. Chem. Soc.*, 2015, **137**, 5549-5554.
64. V. A. Vlaskin, N. Janssen, J. van Rijssel, R. Beaulac and D. R. Gamelin, *Nano Lett.*, 2010, **10**, 3670-3674.

65. E. J. McLaurin, V. A. Vlaskin and D. R. Gamelin, *J. Am. Chem. Soc.*, 2011, **133**, 14978-14980.
66. R. Xu, C. Liao, Y. Xu, C. Zhang, M. Xiao, L. Zhang, C. Lu, Y. Cui and J. Zhang, *Nanoscale*, 2017, **9**, 18281-18289.
67. D. Parobek, B. J. Roman, Y. Dong, H. Jin, E. Lee, M. Sheldon and D. H. Son, *Nano Lett.*, 2016, **16**, 7376-7380.
68. W. Liu, Q. Lin, H. Li, K. Wu, I. Robel, J. M. Pietryga and V. I. Klimov, *J. Am. Chem. Soc.*, 2016, **138**, 14954-14961.
69. K. Xu, C. C. Lin, X. Xie and A. Meijerink, *Chem. Mater.*, 2017, **29**, 4265-4272.
70. S. Das Adhikari, S. K. Dutta, A. Dutta, A. K. Guria and N. Pradhan, *Angew. Chem. Int. Ed.*, 2017, **56**, 8746-8750.
71. X. Yuan, S. Ji, M. C. De Siena, L. Fei, Z. Zhao, Y. Wang, H. Li, J. Zhao and D. R. Gamelin, *Chem. Mater.*, 2017, **29**, 8003-8011.
72. D. Gao, B. Qiao, Z. Xu, D. Song, P. Song, Z. Liang, Z. Shen, J. Cao, J. Zhang and S. Zhao, *J. Phys. Chem. C*, 2017, **121**, 20387-20395.
73. T. Qiao, D. Parobek, Y. Dong, E. Ha and D. H. Son, *Nanoscale*, 2019, **11**, 5247-5253.
74. G. Huang, C. Wang, S. Xu, S. Zong, J. Lu, Z. Wang, C. Lu and Y. Cui, *Adv. Mater. (Weinheim, Ger.)*, 2017, **29**, 1700095.
75. J. Zhu, X. Yang, Y. Zhu, Y. Wang, J. Cai, J. Shen, L. Sun and C. Li, *J. Phys. Chem. Lett.*, 2017, **8**, 4167-4171.
76. F. Li, Z. Xia, Y. Gong, L. Gu and Q. Liu, *J. Mat. Chem. C*, 2017, **5**, 9281-9287.
77. D. Parobek, Y. Dong, T. Qiao and D. H. Son, *Chem. Mater.*, 2018, **30**, 2939-2944.
78. W. J. Mir, Y. Mahor, A. Lohar, M. Jagadeeswararao, S. Das, S. Mahamuni and A. Nag, *Chem. Mater.*, 2018, **30**, 8170-8178.
79. Q. A. Akkerman, D. Meggiolaro, Z. Dang, F. De Angelis and L. Manna, *ACS Energy Lett.*, 2017, **2**, 2183-2186.
80. W. J. Mir, A. Swarnkar and A. Nag, *Nanoscale*, 2019, **11**, 4278-4286.
81. X. Li, Y. Guo and B. Luo, *Crystals*, 2018, **8**, 4.
82. T. Ji, W.-B. Jian and J. Fang, *J. Am. Chem. Soc.*, 2003, **125**, 8448-8449.
83. C. A. Stowell, R. J. Wiacek, A. E. Saunders and B. A. Korgel, *Nano Lett.*, 2003, **3**, 1441-1447.
84. G. Manna, S. Jana, R. Bose and N. Pradhan, *J. Phys. Chem. Lett.*, 2012, **3**, 2528-2534.
85. L. Peng, D. Li, Z. Zhang, K. Huang, Y. Zhang, Z. Shi, R. Xie and W. Yang, *Nano Research*, 2015, **8**, 3316-3331.
86. S. Cao, J. Zheng, C. Dai, L. Wang, C. Li, W. Yang and M. Shang, *J. Mater. Sci.*, 2018, **53**, 1286-1296.
87. G. Zhang, S. Mei, X. Wei, C. Wei, W. Yang, J. Zhu, W. Zhang and R. Guo, *Nanoscale research letters*, 2018, **13**, 170.
88. L. Peng, K. Huang, Z. Zhang, Y. Zhang, Z. Shi, R. Xie and W. Yang, *ChemPhysChem*, 2016, **17**, 752-758.
89. W.-J. Zhang, C.-Y. Pan, F. Cao and X. Yang, *J. Mat. Chem. C*, 2017, **5**, 10533-10542.
90. A. Veamatahau, B. Jiang, T. Seifert, S. Makuta, K. Latham, M. Kanehara, T. Teranishi and Y. Tachibana, *Phys. Chem. Chem. Phys.*, 2015, **17**, 2850-2858.
91. X. Wang, L. Qu, J. Zhang, X. Peng and M. Xiao, *Nano Lett.*, 2003, **3**, 1103-1106.
92. M. M. Krause and P. Kambhampati, *Phys. Chem. Chem. Phys.*, 2015, **17**, 18882-18894.

93. Y. Yang, O. Chen, A. Angerhofer and Y. C. Cao, *Chemistry–A European Journal*, 2009, **15**, 3186-3197.
94. Y. Hefetz, W. Goltsos, A. Nurmikko, L. Kolodziejski and R. Gunshor, *Appl. Phys. Lett.*, 1986, **48**, 372-374.
95. D. Leinen, *Phys. Rev. B*, 1997, **55**, 6975.
96. J. Seufert, G. Bacher, M. Scheibner, A. Forchel, S. Lee, M. Dobrowolska and J. Furdyna, *Phys. Rev. Lett.*, 2001, **88**, 027402.
97. K. Shibata, E. Nakayama, I. Souma, A. Murayama and Y. Oka, *Phys. Status Solidi B*, 2002, **229**, 473-476.
98. H.-Y. Chen, T.-Y. Chen and D. H. Son, *J. Phys. Chem. C*, 2010, **114**, 4418-4423.
99. D. Rossi, D. Parobek, Y. Dong and D. H. Son, *J. Phys. Chem. C*, 2017, **121**, 17143-17149.
100. S. Maiti, H.-Y. Chen, T.-Y. Chen, C.-H. Hsia and D. H. Son, *J. Phys. Chem. B*, 2012, **117**, 4399-4405.
101. R. Beaulac, P. I. Archer, J. van Rijssel, A. Meijerink and D. R. Gamelin, *Nano Lett.*, 2008, **8**, 2949-2953.
102. C.-H. Hsia, A. Wuttig and H. Yang, *ACS Nano*, 2011, **5**, 9511-9522.
103. E. J. McLaurin, L. R. Bradshaw and D. R. Gamelin, *Chem. Mater.*, 2013, **25**, 1283-1292.
104. S. Ithurria, P. Guyot-Sionnest, B. Mahler and B. Dubertret, *Phys. Rev. Lett.*, 2007, **99**, 265501.
105. H.-Y. Chen, S. Maiti, C. A. Nelson, X. Zhu and D. H. Son, *J. Phys. Chem. C*, 2012, **116**, 23838-23843.
106. A. Vink, M. De Bruin, S. Roke, P. Peijzel and A. Meijerink, *J. Electrochem. Soc.*, 2001, **148**, E313-E320.
107. C. S. Erickson, L. R. Bradshaw, S. McDowall, J. D. Gilbertson, D. R. Gamelin and D. L. Patrick, *ACS Nano*, 2014, **8**, 3461-3467.
108. L. R. Bradshaw, K. E. Knowles, S. McDowall and D. R. Gamelin, *Nano Lett.*, 2015, **15**, 1315-1323.
109. H. Xin, J. K. Katahara, I. L. Braly and H. W. Hillhouse, *Adv. Energy Mat.*, 2014, **4**, 1301823.
110. A. A. Bol, J. Ferwerda, J. A. Bergwerff and A. Meijerink, *J. Lumin.*, 2002, **99**, 325-334.
111. B. B. Srivastava, S. Jana and N. Pradhan, *J. Am. Chem. Soc.*, 2010, **133**, 1007-1015.
112. C. Corrado, Y. Jiang, F. Oba, M. Kozina, F. Bridges and J. Z. Zhang, *J. Phys. Chem. A*, 2009, **113**, 3830-3839.
113. R. W. Meulenberg, T. van Buuren, K. M. Hanif, T. M. Willey, G. F. Strouse and L. J. Terminello, *Nano Lett.*, 2004, **4**, 2277-2285.
114. K. E. Knowles, H. D. Nelson, T. B. Kilburn and D. R. Gamelin, *J. Am. Chem. Soc.*, 2015, **137**, 13138-13147.
115. J. Suyver, T. Van der Beek, S. Wuister, J. Kelly and A. Meijerink, *Appl. Phys. Lett.*, 2001, **79**, 4222-4224.
116. G. K. Grandhi, R. Tomar and R. Viswanatha, *ACS Nano*, 2012, **6**, 9751-9763.
117. G. K. Grandhi and R. Viswanatha, *J. Phys. Chem. Lett.*, 2013, **4**, 409-415.
118. K. E. Hughes, K. H. Hartstein and D. R. Gamelin, *ACS Nano*, 2018, **12**, 718-728.
119. P. J. Whitham, K. E. Knowles, P. J. Reid and D. R. Gamelin, *Nano Lett.*, 2015, **15**, 4045-4051.
120. S. Gul, J. K. Cooper, C. Corrado, B. Vollbrecht, F. Bridges, J. Guo and J. Z. Zhang, *J. Phys. Chem. C*, 2011, **115**, 20864-20875.

121. S. Gul, J. K. Cooper, P.-A. Glans, J. Guo, V. K. Yachandra, J. Yano and J. Z. Zhang, *ACS Nano*, 2013, **7**, 8680-8692.
122. B. Car, S. Medling, C. Corrado, F. Bridges and J. Z. Zhang, *Nanoscale*, 2011, **3**, 4182-4189.
123. A. M. Jawaid, S. Chattopadhyay, D. J. Wink, L. E. Page and P. T. Snee, *ACS Nano*, 2013, **7**, 3190-3197.
124. H. D. Nelson, X. Li and D. R. Gamelin, *J. Phys. Chem. C*, 2016, **120**, 5714-5723.
125. R. Viswanatha, S. Brovelli, A. Pandey, S. A. Crooker and V. I. Klimov, *Nano Lett.*, 2011, **11**, 4753-4758.
126. G. Pan, X. Bai, D. Yang, X. Chen, P. Jing, S. Qu, L. Zhang, D. Zhou, J. Zhu, W. Xu, B. Dong and H. Song, *Nano Lett.*, 2017, **17**, 8005-8011.
127. T. J. Milstein, D. M. Kroupa and D. R. Gamelin, *Nano Lett.*, 2018, **18**, 3792-3799.
128. T. J. Milstein, K. T. Kluherz, D. M. Kroupa, C. S. Erickson, J. J. De Yoreo and D. R. Gamelin, *Nano Lett.*, 2019, **19**, 1931-1937.
129. X. Luo, T. Ding, X. Liu, Y. Liu and K. Wu, *Nano Lett.*, 2019, **19**, 338-341.
130. P. Vergeer, T. J. H. Vlugt, M. H. F. Kox, M. I. den Hertog, J. P. J. M. van der Eerden and A. Meijerink, *Phys. Rev. B*, 2005, **71**, 014119.
131. B. M. van der Ende, L. Aarts and A. Meijerink, *Phys. Chem. Chem. Phys.*, 2009, **11**, 11081-11095.
132. R. T. Wegh, H. Donker, K. D. Oskam and A. Meijerink, *Science* 1999, **283**, 663-666.
133. W. Shao, C.-K. Lim, Q. Li, M. T. Swihart and P. N. Prasad, *Nano Lett.*, 2018, **18**, 4922-4926.
134. F. Wang and X. Liu, *Chem. Soc. Rev.*, 2009, **38**, 976-989.
135. L. R. Bradshaw, A. Hauser, E. J. McLaurin and D. R. Gamelin, *J. Phys. Chem. C*, 2012, **116**, 9300-9310.
136. H.-Y. Chen, T.-Y. Chen, E. Berdugo, Y. Park, K. Lovering and D. H. Son, *J. Phys. Chem. C*, 2011, **115**, 11407-11412.
137. M. A. White, A. L. Weaver, R. Beaulac and D. R. Gamelin, *ACS Nano*, 2011, **5**, 4158-4168.
138. P. K. Santra and P. V. Kamat, *J. Am. Chem. Soc.*, 2012, **134**, 2508-2511.
139. J. Tian, L. Lv, C. Fei, Y. Wang, X. Liu and G. Cao, *J. Mater. Chem.*, 2014, **2**, 19653-19659.
140. G. Halder and S. Bhattacharyya, *J. Phys. Chem. C*, 2015, **119**, 13404-13412.
141. J. Luo, H. Wei, Q. Huang, X. Hu, H. Zhao, R. Yu, D. Li, Y. Luo and Q. Meng, *Chem. Commun.* , 2013, **49**, 3881-3883.

TOC

This work discusses the photophysical pathways in doped quantum dots responsible for generating photons of non-exciton origin and hot electrons.

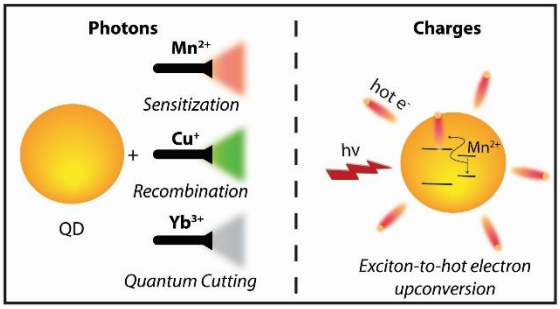

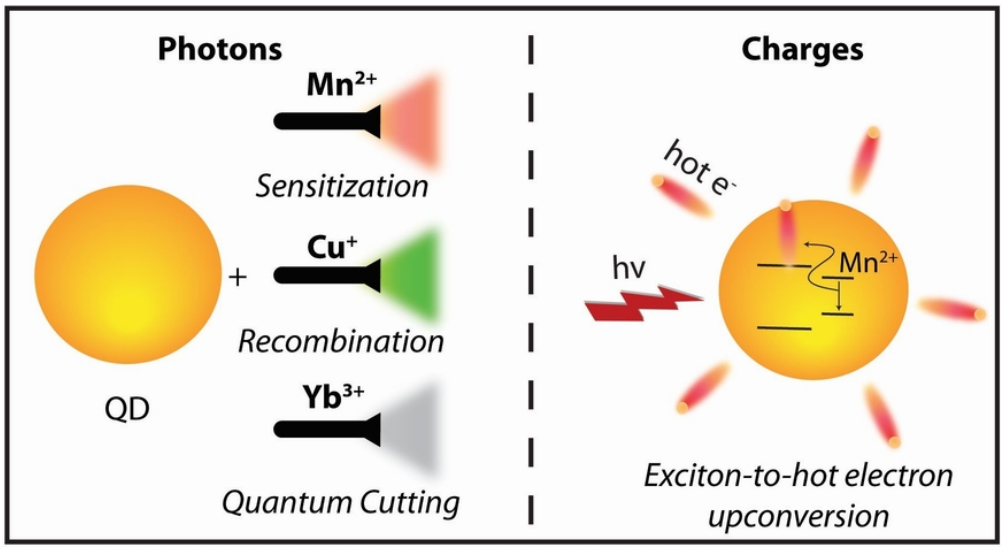

73x39mm (300 x 300 DPI)